Eng. & Technology, Vol.25, No.1, 2007

Finite Element Analysis of the Rake Angle Effects on Residual Stresses in a Machined Layer

Dr. Maan Aabid Tawfiq*
Received on: 9/2/2005
Accepted on: 18/7/2005

Abstract
In this paper, a plane strain Finite Element Method is developed and applied to model and simulate the orthogonal metal cutting of (AISI 1045 St) with continuous chip formation. Seven sets of simulation results for cutting with rake angles (-15°, -10°, -5°, 0°, 5°, 10 ° and 15°), are summarized and compared to analyze their effects in the cutting process in steady state condition. Simulation results of the residual stresses below the machined layer are presented and compared with other papers in the literature and showed good agreement.
Simulation results offer an insight into residual stresses through different values of rake angles. Based on simulation results, characteristics of residual stress distribution can be controlled by optimizing the rake angle. The simulated results show that for positive rake angles and position, the zero of maximum effective stress is found to be at (0.04) mm beneath the work piece surface, while for negative rake angles, the position of maximum effective stress is changed to be directly on the workpiece surface.

تأثير زاوية جرف عدة القطع على الاجهادات المتبقية في الطبقة المشغلة باستخدام طريقة العناصر المحددة

الخلاصة
تم في هذا البحث تطبيق طريقة العناصر المحددة(Finite Element Method) بالانفعال المستوي، وذلك بهدف نمذجة ومحاكاة عملية القطع العمودي لصلب نوع (AISI 1045 St)، وذلك عند ظروف تكوين النحاتة المستمرة (continuous chip). تم تهيئة نماذج تحاكي سبعة قيم لزوايا جرف عدة القطع وهي: (- ١٥°، -١٠°، -٥°، ٠°، ٥°، ١٠°،-١٥°)، وذلك بهدف تحليل ومقارنة تأ ثير هذه الزاوية تحت ظروف قطع مستقرة على الاجهادات المتبقية أمكن باستخدام طريقة العناصر المحددة توضيح الاجهادات المتبقية والناتجة عن عملية القطع وذلك في المنطقة الواقعة أ سفل الطبقة المشغلة وتم كذلك مقارنة النتائج المستحصلة مع بحوث أخرى منشورة في الأدبيات و أعطت نتائج جيدة، كما وبينت النتائج وصفا دقيقا لتأثيرات زاوية الجرف على الاجهادات المتبقية، حيث أظهرت نتائج المحاكاة امكانية السيطرة على قيم وتوزيع هذه الاجهادات من خلال التحكم الأمثل بقيم زاوية الجرف. وأظهرت نتائج المحاكاة كذلك بانه عند زوايا الجرف ذات القيم الموجبة والصفر يكون موقع أقصى اجهاد فعال عند مسافة تبعد مقدار (٠,٠٤) ملم عن حافة السطح المشغل، في حين تتغيرقيم أقصى اجهاد فعال عند زوايا الجرف ذات القيم السالبة لتكون على حافة السطح المشغل تماما.

*Dept. of Production Eng. & Metallurgy, UOT., Baghdad, IRAQ.

https://doi.org/10.30684/etj.25.1.6
2412-0758/University of Technology-Iraq, Baghdad, Iraq

1. Introduction

The plain strain orthogonal metal cutting process, with the direction of relative movement of the wedge-shaped cutting tool perpendicular to its straight cutting edge, has been extensively studied, since it provides a reasonably good modeling of the chip formation on the major cutting edge of many metal removal processes such as turning, milling, drilling, grinding, etc. Numerical simulation of machining processes can be traced back to the early seventies, when Finite Element models for continuous chip formation were proposed. The advent of fast computers and development of new techniques to model large plastic deformations have favored machining simulation. One of the important parameters in the orthogonal metal cutting process is the rake angle between the face of the cutting tool and the plane perpendicular to the cutting direction [1, 2]. The magnitude of rake angle has significant effects on the performance of the cutting tool and the surface integrity of the sub-layer generated by the machining process and its effects on the residual stresses. The residual stresses on the machined surface are important factor in determining the performance and fatigue strength of mechanical components. The FEM has been developed and applied to predict the distributions of the residual stresses in orthogonal metal cutting and compared with X-ray diffraction measurement [3,4], as shown in Fig.(1). The residual stresses and surface finish can significantly affect the resistance of material to failure when subjected to high cycle fatigue loads. The fatigue crack, in general, initiates at the surface of the components and propagates into the material. Understanding and controlling the variance of fatigue life are essential to achieve this goal, since fatigue is their predominant mode of failure. An important way to understand the variance of fatigue life is to build models capable of predicting this information accurately [5]. If the surface residual stress is tensile and further tensile stresses are applied, then due to the loading fatigue resistance may be significantly reduced. ***Henriksen*** [6] stated that the main residual stress in the work material is caused by the machining, which induced the plastic deformation of a surface layer. Furthermore, the geometrical accuracy of the components will also be influenced by the residual stress distribution. Currently, the determination of residual stresses heavily depends on experimentation. However, experimental approach has many limitations for example: time consuming and labor intensive, accuracy of measurement depends on operator skill and machine capacity. Therefore, developing a methodology capable of accurately predicting machining induces residual stress is of great value. ***Lio et al***. [7] stated that the prediction of machining induced residual stress is sensitive to the coefficient of friction at the tool chip interface region. It is generally believed that residual stresses result from plastic deformation, thermal stress and phase transformation of the machined layer. ***Liu*** [8] showed that, residual stresses in high performance alloys and steels are

of considerable industrial importance because they can affect failure by fatigue, creep or cracking. ***Liu and Barash*** [9] showed that mechanical deformation of the workpiece surface is the one of the causes of producing both tensile and compressive residual stresses in machining. ***Kono et al***. [10] presented findings that residual stress increases with the cutting speed but does not monotonically change with the depth of cut in hard turning. ***Schreiber and Schlicht*** [11] confirmed that the mechanical properties of the workpiece material to be machined have a great influence on the magnitude and distribution of the residual stresses. ***Matsumoto*** [12] concluded that material hardness has a significant effect on the pattern of residual stress that remains in the mechanical part.

Tonshoff et al. [13] found that the residual stresses are influenced by both the cutting speed and the tool wear because increasing the cutting speed will accelerate the tool wear. This paper further addresses the rake angle effects on residual stresses at the machined layer and its distribution in order to select the optimum rake angle and study in detail the patterns of residual stress distribution and its behavior. **Xiaoping et al** [14] studied the relation between the simulated stress profiles and showed how the residual stresses are varied along the distance below the machined surface, as shown in Fig.(2). **Ship** [15] showed the trends of both the tensional stresses (σ_x) (x-stress), which is in the cutting direction, and (σ_y)(Y-stress), which is perpendicular to the cutting direction. The residual stress profiles are plotted as a function of depth into the workpiece as shown in Fig.(3).

2.Finite Element Modeling Approach

Two special FEM explicit codes (MSC FEA/Patran/V 2004 & MSC FEA/Dytran/V 2004) are used to model the chip formation process. The codes are applied with certain modifications to suit orthogonal metal cutting principles. The first code is used for preprocessing and postprocessing, while the second one is used for the analysis stage. This selection is due to the explicit method is originally developed to analyze high-speed dynamic events that are extremely costly to analyze when using implicit programs, such as ABAQUS/standard code. The explicit codes hare also advantages over the implicit method in modeling complex contact problems and materials with degradation and failure, which is essential to model a metal cutting process. The orthogonal metal cutting process was modeled into three parts:

2.1 Orthogonal Cutting Modeling

Solid modeling is done for the proposed model sets in order to imitate orthogonal cutting, including in general the mesh selection to a number of elements, nodes and the boundary conditions. Two types of Lagrangian elements are applied. The first element is (8) nodes, called (CHEXA), and is used for Lagrange solid elements to simulate the deformed material (workpiece), which has six degree of freedom per node: translational and rotational in x, y and z directions. This element comes with hourglass control that is important in dealing with large

deformation, such as metal cutting. The other element is (4) nodes, called (CQUAD4), and is used for shell elements with three degree of freedom per node: translation in the nodal x, y and z directions, to simulate the shell between the chip and workpiece, in order to be used for tying them under predetermined constant force criteria. The boundary conditions are such that the tool can move freely in x-direction, which in other degree of freedom is restricted. The bottom element of the workpiece is restrained from moving in all directions, as shown in Figure (4). The metal machined in this simulation is (AISI 1045 St.), whose physical and thermal properties and constants needed for the specified FEM program are available in the mentioned codes[16, 17] and being shown in tables (1and 3).

Since most tool materials have significantly high elastic modulus, compared with large plastic deformation of workpiece, the elastic deflection of the cutting tool can be ignored. The cutting tool is assumed to be perfectly rigid with seven rake angles: (-15^o,-10^o,-5^o, 0^o, 5^o, 10^o and 15^o). The cutting conditions and other tool geometry are shown in table (2).

Other assumption for the modeling include: the chip formation is continuous, the workpiece is stress free prior to the cutting operation, and that cutting tool wear, residual stress from phase transformation are ignored, and the cutting is performed in air with no liquid coolant.

2.2 Friction Modeling

In metal cutting process, it is generally observed that the mean coefficient of friction on the tool face varies considerably with the change in cutting speed, rake angle and so on. This results from the extreme conditions of metal cutting area, where the normal pressure at the tool-chip interface is very high. The contact surfaces in our model are assumed to be sliding and sticking zones due to reference [18]. A new model of friction is applied called a rate dependent Coulomb friction (μ), which is expressed by the following relation [16]:

$$\mu = \mu_k + (\mu_s - \mu_k) e^{- \beta' v}$$

where: μ_s = static coefficient of friction.

μ_k= kinetic coefficient of friction.

β'= exponent decay coefficient.

v = relative sliding velocity of the slave and master surfaces.

The optimum coefficients of friction is determined by iterating the finite element simulations until acceptable agreement is reached through trial and error numerical tests, the optimum static and kinetic coefficient of friction are found to be (0.4& 0.5) respectively,and are estimated using ***Zorev's*** stress distribution model [18], which is till now, the most extensive experimental model for friction estimation in metal cutting field.

2.3 Material Modeling

The orthogonal cutting model is modeled with two different types of material models, one for the tool and another for the workpiece. The tool was assumed to be perfectly experiences no wear and rigid, so it was modeled as perfectly elastic solid. For the workpiece material, due to the large plastic deformation subjected in metal

cutting process, the workpiece material strain hardens. The isotropic hardening model is employed to model this behavior by defining flow stress as a function of plastic strain, strain rate and temperature. The following ***Johnson-Cook*** constitutive model was able to include the effective plastic strain, strain rate and the strain hardening effects under high machining temperature [16]:

$$\sigma=(A+B\bar{\varepsilon}^{n})(1+C\ln\dot{\varepsilon}^{*})(1-\mathbf{T}^{*m})$$

where:

$\dot{\varepsilon}^{*}$= the non dimensional effective strain rate = ($\dot{\varepsilon}$ / $\dot{\varepsilon}_{o}$)

T*= the non dimensioned temperature=($\mathbf{T}$ - $\mathbf{T_o}$)/($\mathbf{T}_{melt}$–$\mathbf{T_o}$). $\bar{\varepsilon}$ = the effective plastic strain. $\dot{\varepsilon}$ = the effective strain rate.

$\dot{\varepsilon}_{o}$ = the reference strain rate.

$\mathbf{T}$ = the working temperature.

$\mathbf{T_o}$ = the room temperature.

$\mathbf{T}_{melt}$ = the melting temperature.

A, *B*, C, ***n,*** and *m* are material parameters.

Table (3) shows ***Johnson-Cook*** parameters for (AISI 1045 St). These parameters are obtained for various materials found in the ***Johnson-Cook*** paper and from experimental data [19, 20]. In this model the metal is assumed to be homogeneous, isotropic and incompressible solid

3.Discussion

Fig.(4) shows an example of one of the seven models created for this study, (at rake angle of 5º). The Finite Element model, mesh and chip formation process are shown during the steady state condition.The model shows the deformed chip and the effective stresses at both the primary and secondary deformation zones. Also the residual stresses are shown in detail along the machined layer, the simulated results show the residual stresses on a section (A-A) of the workpiece surface in (X and Y) directions, both the tensional stresses (σ_x) (x-stress), which is in the cutting direction, and (σ_y)(Y-stress), which is perpendicular to the cutting direction. The residual stress profiles are plotted as a function of depth into the workpiece. The profiles typically decay to zero around (0.225) mm. beneath the workpiece surface, varying from positive to negative in order to satisfy equilibrium.Fig.(5) shows family of predicted effective residual stress profiles as a function of depth into the workpiece for various rake angles. As the rake angle is varied from (-15^{o} to 15^{o}), the effective residual stress changes to decrease, since the cut surface with smaller rake angle generates more significant distortion of elements. Thicker chips, smaller shear angle and longer contact length are recorded using the cutting tool with smaller rake angles. A stagnant chip material ahead of the tool tip is noticed, which is always observed with large negative rake angles and is assumed to act like a stable built-up edge. The curves trend shown in this figure is similar to the distribution of residual stresses for different rake angles when compared with experimental X-ray diffraction measurement and other FEM tests being shown in Fig.(1) and Fig.(2) in references[4,14] respectively.

Fig.(6) shows the simulated residual stress on section (A-A) under seven

different tool rake angle conditions. In Fig. (6-A), at the rake angle of (-15^o), the tensile stress (σ_x) is (30) MPa and gradually increases to (50) MPa at (0.04) mm beneath the work piece surface, then it transforms into compressive stress beneath the machined surface with a maximum value of (-130) MPa. As for the residual stress (σ_y), its maximum value on the workpiece surface is (-850) MPa. The maximum effective stress appears on the workpiece surface, with a maximum value of (900) MPa. The effective stress also decreases as its distance from the workpiece surface increases. Fig.(6-B and C), shows similar trends of the variation of residual stresses for the rake angle values of (-10^o and -5^o), but the values of (σ_x) for tensile values is increased from(70-90) MPa as the rake angle is increased from (-10^o to -5^o),while the compressive values (σ_y) is decreased from (-750 to- 680) MPa. Also the residual effective stresses decreased when the rake angle is increased in this region (-10^o to -5^o), but the position of maximum effective stress stays the same as in Fig.(6-A). i.e. at (0.04) mm beneath the work piece surface. Fig.(6-D,E,F and G), show that the maximum values of effective residual stresses continuously decreases for the rake angle (0^o,5^o,10^o,15^o), from (770, to 550)MPa, but the position of maximum effective stress is changed here to be directly on the workpiece surface. the values of (σ_x) for maximum tensile values is increased from (110, 130, 160, 200) MPa for rake angles (0^o, 5^o, 10^o, 15^o) respectively, the position of transform from positive to negative for this region of rake angles is at (0.05-0.075)mm beneath the workpiece surface. The maximum compressive values (σ_y) is decreased from (-700, -700, -600 and -500), for rake angles (0^o, 5^o, 10^o, 15^o) respectively in comparison with our current work. Fig.(3)shows similar trends of residual effective stresses, tensile and compressive stresses for rake angle(5^o)[15]. The mentioned description of residual stress distribution is similar and agreed well with the experimental tests being published in reference [14,21].

4 –Conclusions

The following main conclusions may be drawn from the present simulation work:

1. The residual stress distribution on the workpiece surface is fairly modeled taking into consideration thermal effects and friction conditions using FEM.
2. The tool rake angle has a great effect on residual stress values and its distribution along the machined layer, so the selection of optimum tool rake angle will be easier according to FEM.
3. Under steady state conditions, the residual stress (σ_x), in the cutting direction increases as the rake angle is increased in the range of (-15^o to 15^o).
4. Under steady state conditions, the residual stress (σ_y) perpendicular to the cutting direction is decreased, as the rake angle is increased in the range of (-15^o to 15^o).
5. For positive rake angles and zero (0^o, 5^o, 10^o, 15^o), the position of maximum effective stress is to be directly on the workpiece surface.

And the position of transform from positive to negative residual stress for (σ_x), is at (0.05-0.075) mm beneath the workpiece surface.

6. For negative rake angles (-15°, -10°, -5°), the position of maximum effective stress stays at (0.04) mm beneath the piece work surface. And the position of transform from positive to negative residual stress for (σ_x), is at (0.05-0.06) mm, beneath the workpiece surface.
7. The results of FEM modeling in which the actual experimental results obtained in experimental tests were utilized fully support the results of the analytical modeling.

Reference

1- M. C. Shaw, Metal Cutting Principles, Clarendon Press, Oxford, 1984.

2- G.Boothroyd and W.A. Knight, Fundamentals of machining and machine tools, 2nd edition, Marcel Dekker, New York, 1989.

3- A. J. Shih and H.T. Yang, Experimental and Finite Element predictions of residual stresses due to orthogonal metal cutting, Int. J. Num. Methods in Engineering,Vol.36,pp.1487-1507 , 1993.

4- A. J. Shih, Finite element analysis of the rake angle effects in orthogonal metal cutting, Int. J. Sci., Vol.38, No.1, pp.1-17, 1996.

5- Yang Xiaoping,A methodology for predicting the variance of fatigue life incorporating the effects of manufacturing processes, Ph.D.Thesis,PurdueUniversity, 2001.

6- E.K. Henriksen, Residual stresses in machined surfaces, Trans. ASME, pp.69-76, 1955.

7- Lio C.R., Y.B. Guo, Finite element analysis of the effect of sequential cuts and tool-chip friction on residual stresses in a machined layer, International Journal of Mechanical Sciences, Vol.42, pp.1069-1086, 2000.

8- C.R. Liu, S. Mittal, Single step superfinish hard machining feasibility and feasible cutting conditions, Journal of Robotics and Computer-integrated Manufacturing,Vol.12, No.1, pp.15-27, 1996.

9- C.R. Liu, M.M. Barash, Variables governing patterns of mechanical residual stress in a machined surface, Transactions of the ASME, Journal of Engineering for Industry,Vol.104,No.3,pp.257-264, 1982.

10- Y. Kono, A. Hara, S.Yazu, Uchida T., Mori Y., Cutting performance of sintered CBN tools, Cutting tool materials, Proceedings of the International Conference, American Society for Metals, Ft. Mitchell, Kentucky, September15-17, pp. 218-235, 1980.

11- E. Schreiber and H. Schlicht, Residual stresses after turning of hardened components, The International Conference on Residual stresses, Garnish Partenkirchen(FRG), pp.853-860, 1986.

12- Wu D.W, Matsumoto Y., The effect of hardness on residual stresses in orthogonal machining of AISI 4340 steel., Transactions of the ASME, Journal of Engineering for Industry, Vol.112, No.(3), pp.245-252, 1990.
13- H.K. Tonshoff, H.G. Wobker, Brandt D. Tribological aspects of hard turning with ceramic tools, Journal of the Society of Tribologists and Lubrication Engineers,Vol.51,No.(2),pp.163-168, 1995.
14- Xiaoping Yang, C, Richard Liu, A new stress-based model of friction behavior in machining and its significant impact on residual stresses computed by finite element method, International Journal of Mechanical Sciences, Vol.44, pp.703-723, 2002.
15- Ship Peng Lo, An analysis of cutting under different rake angles using finite element method, Journal of Materials Processing Technology, Vol.105, pp.143-151, 2000.
16- User's Manual of MSC FEA/DYTRAN/Version/2004,MSC /Software, Corporation, 2004.
17- User's Manual of Ansys, Version 8.1, 2004.
18- Zorev, N. N., Metal cutting Mechanics, Pergamon Press, Oxford, 1966.
19- Tugrul Ozel, Erol Zeren, Determination of work material flow stress and friction for FEA of machining using orthogonal cutting tests, journal of material processing technology, Article in press, pp.1-7, 2004.
20- S.P.Jaspers,J.H.Dautzenberg, Material behavior in conditions similar to metal cutting in the primary shear zone, J. Mater. Process. Technology,Vol.122,pp.322-330, 2002.
21- V. Kalhori, Modeling and simulation of mechanical cutting, Doctoral thesis, Lulea University of Technology, Lulea, Sweden, 2001.

Table (1): Chemical composition of (AISI 1045 St).

% C	% Si	% Mn	% P	% S
0.47	0.24	0.7	0.007	0.029

Table (2): Simulation Cutting conditions and cutting tool geometry.

Clearance angle	Cutting speed (m/min)	Uncut chip thickness (mm)	Depth of cut (mm)	Nose radius (mm)	Initial temperature
7^{o}	200	0.5	0.5	0.045	$25\,^{o}C$

Table (3): ***Johnson-Cook*** parameters for (AISI 1045 St).

Static yield stress **(A)**	**553.1 MPa**	Strain Hardening exponent **(n)**	**0.234**
Hardening parameter **(B)**	**600.8 MPa**	Temperature exponent **(m)**	**1.0**
Strain rate parameter **(c)**	**0.0134 sec^{-1}**	Melting temperature **(T_{melt})**	**1500 °C**
Reference strain rate **(ε̇)**	**1.0 sec^{1}**	Room temperature **(T_o)**	**25 ° C**

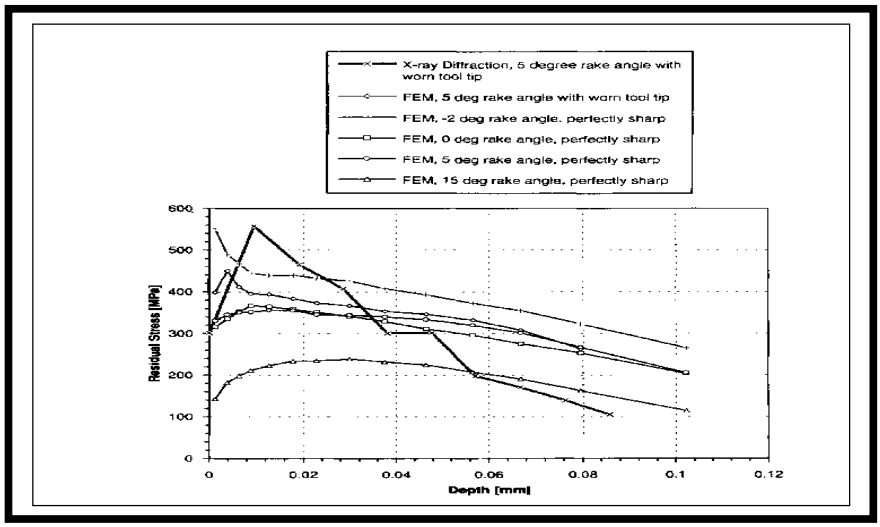

Fig.(1): The distribution of residual stresses in the cutting direction for different rake angles and the comparison with X-ray diffraction measurement and FEM, Ref.[4].

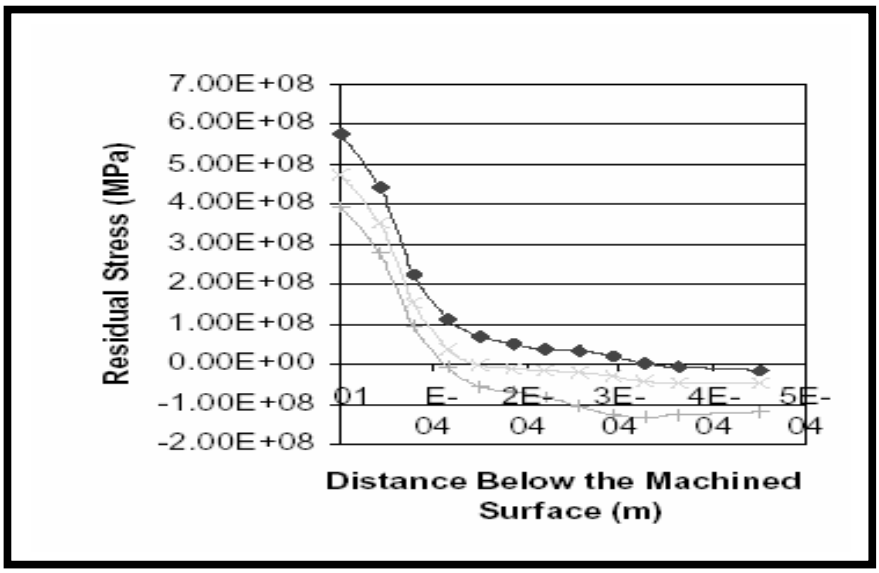

Fig.(2): Simulated residual stress profiles as shown by Ref.[14].

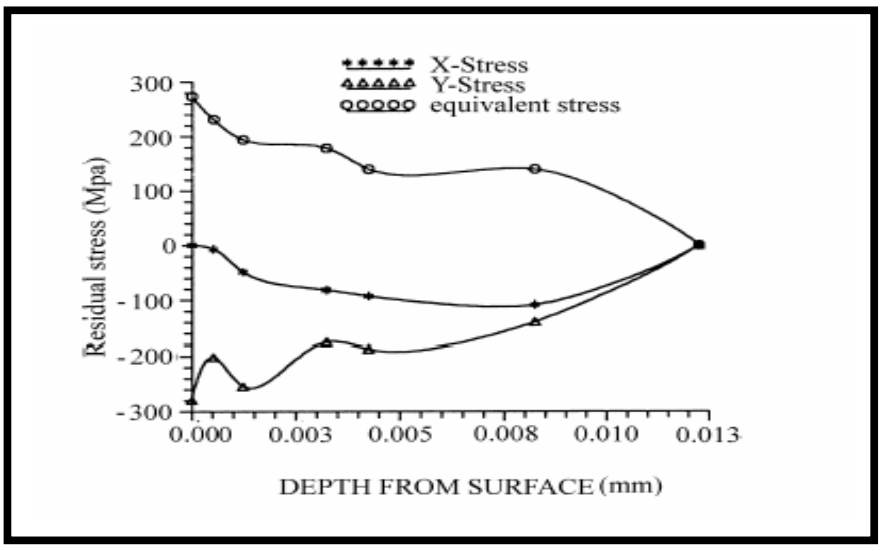

Fig.(3): Simulated residual stress profiles as shown by Ref.[15].

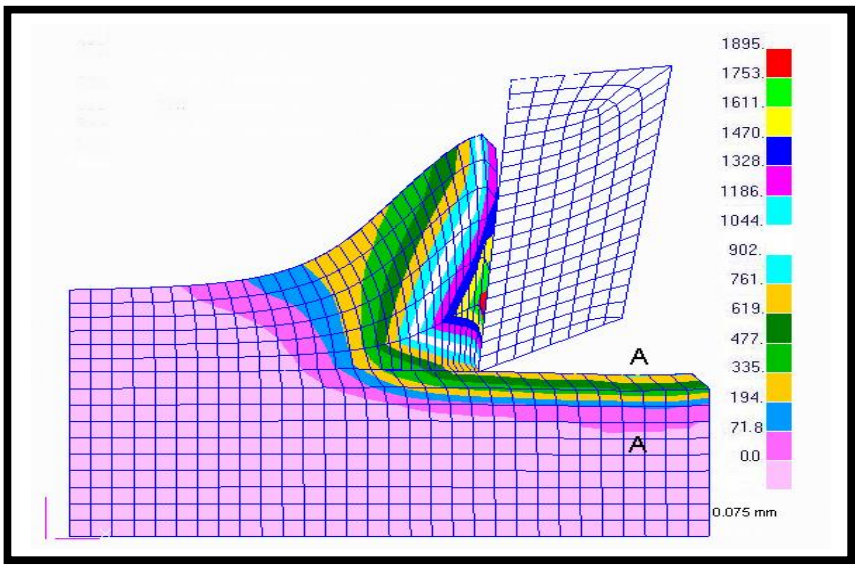

Fig.(4): FEM model simulation characteristics. Showing the effective residual stresses and its distribution over the deformation zones and machined surface, rake angle = 5^{o}.

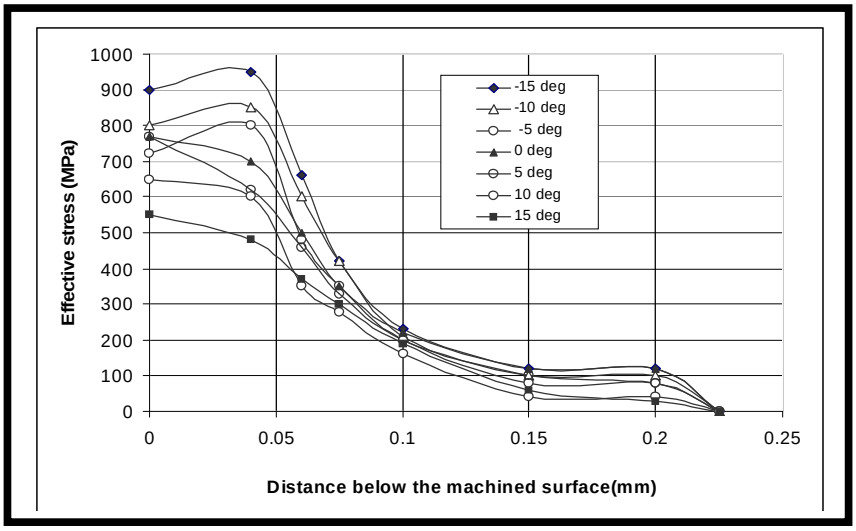

Fig.(5): Family of predicted residual stress profiles as a function of depth into the workpiece for various rake angles.

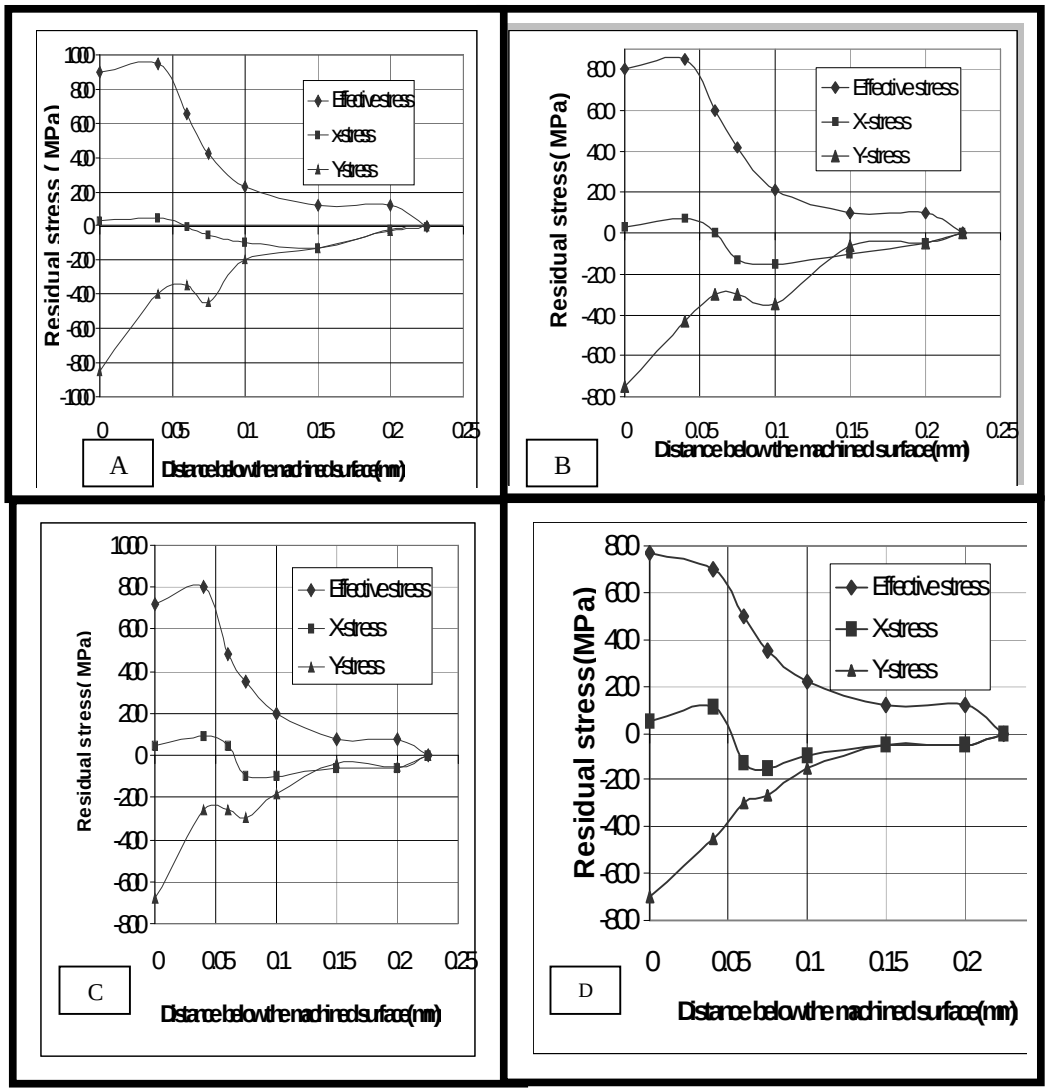

Fig. (6-A): The distribution of residual stresses for different tool rake angles.(**A = -15^{O} , B = -10^{O}, C = -5^{O}, D = 0^{O})**

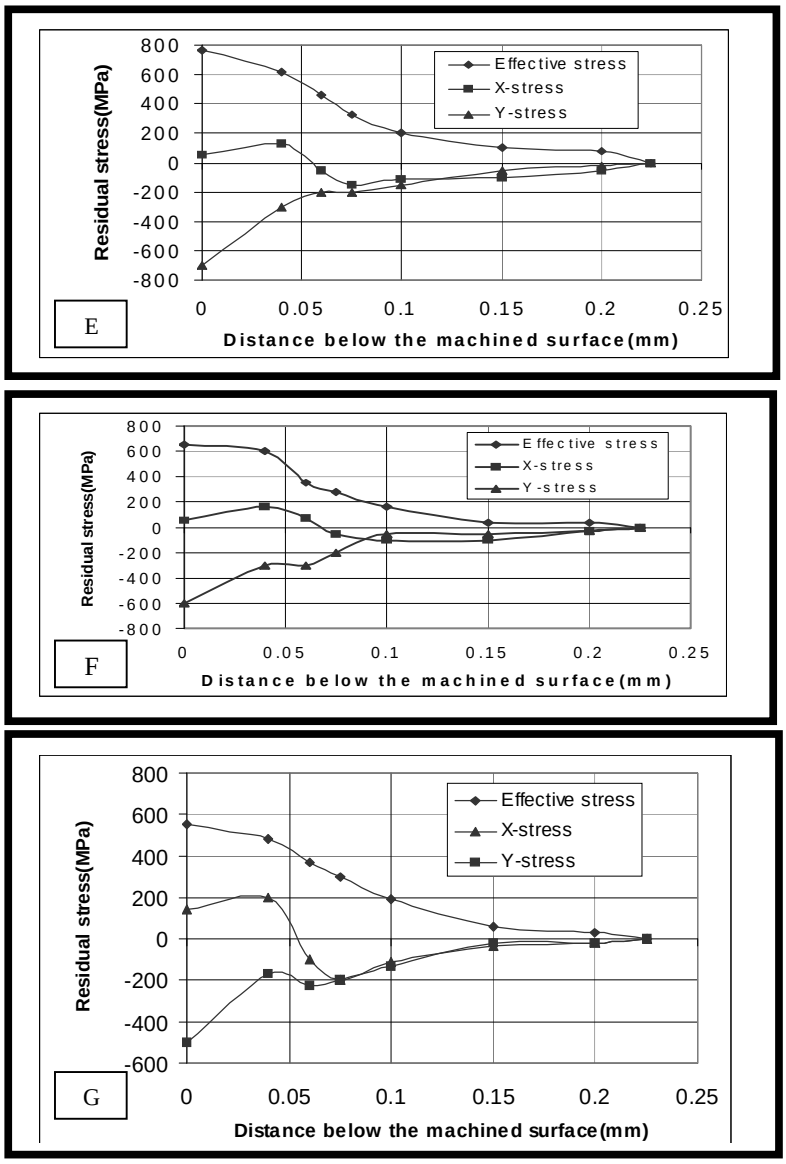

Fig. (6-B): The distribution of residual stresses for different tool rake angles **(E = 5^{O}, F = 10^{O}, G = 15^{O}).**